MAGNETIC PROPERTIES OF TERNARY LAYERED $TlGa_{0.977}Fe_{0.023}Se_2$ DILUTE MAGNETIC SEMICONDUCTOR CRYSTAL

FAIK MIKAILZADE [1*], SERDAR GÖKÇE [1], TOFIG G. MAMMADOV [2], ARZU I. NAJAFOV [2], SAVAŞ BERBER [1], MIRHASAN YU. SEYIDOV [1]

[1] Department of Physics, Gebze Technical University, Gebze, Kocaeli, 41400, Türkiye

[2] Institute of Physics, Ministry of Science and Education, Javid avenue 131, Baku, Azerbaijan

**E - mail address: faik@gtu.edu.tr*

The results of the magnetization studies of Fe doped $TlGaSe_2$ ($TlGa_{1-x}Fe_xSe_2$) layered magnetic semiconductor grown with $x = 0.023$ are presented. The positive value of the Curie temperature together with the observed antiferromagnetic hysteresis loops as well as with the characteristic temperature dependence of magnetic susceptibility indicates the existence of combined antiferromagnetic and weak ferromagnetic ordering between interacting unpaired spin orbitals of Fe^{3+} ions in $TlGa_{1-x}Fe_xSe_2$ compounds. Structural stability, electronic and magnetic properties of the Fe – doped $TlGaSe_2$ four – layer slab were explored using density-functional theory (DFT) calculations. It has been found that substituting Fe single dopant atom at the Ga site, and the formation of substitutional $FeSe_4$ complexes due to the strong hybridization between the electronic states of the dopants and the neighboring Se atoms are geometrically and energetically favorable for $TlGa_{1-x}Fe_xSe_2$. The calculations revealed that the magnetic coupling between Fe dopants and the neighboring Se atoms is dominantly ferromagnetic, while weakly antiferromagnetic interactions between Fe – Fe dopants due to the super - exchange mechanism is favorable.

Keywords: Diluted magnetic semiconductors; dopant stability, magnetic exchange coupling, density functional theory, ferromagnetism, antiferromagnetism.
PACS: 73.20.Dx, 75.30.Et, 78.20.Ls, 68.55.Bd. 1

1. INTRODUCTION

Diluted magnetic semiconductors (DMS), where transition metal ions are substituted for the nonmagnetic ions of the host semiconducting material, have attracted considerable interest in recent decades because of their huge potential for applications in spintronics, which studies electronic devices based on the charge of carriers and spins [1–4]. The development of DMS materials with Curie temperature above the room temperature is the key challenge in the establishment of materials for applications in spintronic devices.

In the present paper, the results of the studies of the effect of incorporation of Fe atoms in bulk $TlGaSe_2$ layered semiconducting crystals instead the gallium substitutional site inside $Ga^{3+}Se_4^{2-}$ framework are presented. $TlGaSe_2$ is a native p – type semiconductor with a direct bandgap of $\sim$ 2.1 – 2.2 eV having monoclinic space group of $C_{2h}^6 - C2/c$ at room temperature with the following unit cell parameters: $a = 10.772$ (3) Å, $b = 10.771$ (5) Å, $c = 15.63$ Å, and $\beta = 100°$ [5–7]. The layered crystal structure of $TlGaSe_2$ is composed from the stacking of metal - chalcogen anionic layers in the ab - plane which is perpendicular to the pseudo tetragonal symmetry c^*- axis of the unit cell. Each layer consists of Ga_4Se_{10} polyhedra built adamantine like by corner - connected four $GaSe_4$ tetrahedrons which are bounded together via sharing Se atoms at the common corners. Succeeding layers are stacked along c^*- axis by alternately turning away with 90° and shifted a quarter of a unit along [110] and [1$\bar{1}$0] directions forming trigonal prismatic voids where Tl^+ ions are located [5].

The first objective of this work is to grow Fe – diluted $TlGaSe_2$ single crystal in which magnetic Fe^{3+} impurities are substituted for Ga cation vacancy sites with concentration of ~ 2.3 %. Then the temperature dependence of magnetic susceptibility in zero field cooled (ZFC) and field cooled (FC) regimes as well as the magnetization M versus the magnetic field H curves ($M(H)$ curves) were measured between ~ 10 and ~ 400 K in the present work. To confirm the crystal structure of the Fe – modified $TlGaSe_2$ compound X - ray diffraction (XRD) – analysis and scanning electron microscopy energy dispersive spectroscopy (SEM-EDX) were carried out. Based on the measured data, we will discuss the origin of the magnetic ordering in $TlGa_{1-x}Fe_xSe_2$ magnetic semiconductor.

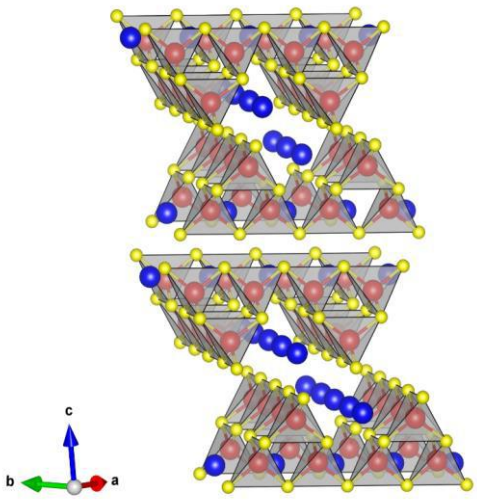

Fig. 1. Visualization of the crystal structure of $TlGaSe_2$ compound composed of $GaSe_4$ tetrahedrons. The blue, red and yellow spheres represent Tl, Ga and Se ions, respectively.

131, H.Javid ave, AZ-1143, Baku
Institute of Physics
E-mail: jophphysics@gmail.com

2 . EXPERIMENTAL TECHNIQUES

$TlGa_{1-x}Fe_xSe_2$ single crystals were grown with the classical vertical Bridgman - Stockbarger technique. The chemical composition of as – prepared Fe – substituted $TlGaSe_2$ single crystals was determined by using scanning electron microscope *Philips XL 30 SFEG* equipped with energy dispersive X - ray (EDX) spectrometer. EDX measurements were taken point to point on the surface of layer at 30 kV.

Magnetization measurements have been performed by using VSM Magnetometer (PPMS, Quantum Design Corporation) for parallel (H ∥ ab) and perpendicular (H ⊥ ab) alignment of the applied magnetic field with respect to the layer plane in the temperature range of between ~ 10 K and ~ 400 K. The magnetization versus temperature measurements have been performed consecutively in ZFC and FC regimes. In ZFC regime the sample was cooled without applying the magnetic field and then the magnetization values (M) were recorded by raising the temperature up to ~ 400 K under the weak magnetic field of H = 50 Oe and the high magnetic field of H = 5 kOe for parallel alignment. In FC regime the sample is cooled to 10 K under the application of the magnetic field of H = 50 Oe and H = 5 kOe for parallel orientation and then the magnetization values (M) are recorded during heating the sample up to ~ 400 K under the same values of applied magnetic field. For perpendicular alignment, ZFC and FC measurements are performed only by applying the weak magnetic field of H = 50 Oe. Isothermal magnetization versus magnetic field curves were recorded during FC measurements for externals fields between - 20 and 20 kOe.

Structure optimization and spin polarized electronic structure calculations of Fe-doped $TlGaSe_2$ have been performed using density functional theory (DFT) [8,9], employing Perdew-Burke-Ernzerhof (PBE) exchange correlation functional within the Generalized Gradient Approximation (GGA) [10]. In the 2x2x1 supercell of $TlGaSe_2$, we substituted an Fe atom for Ga to simulate the Fe-doped $TlGaSe_2$. Our supercell has 128 atoms, and one out of 32 Ga atoms is substituted, corresponding to x=0.03125 in $TlGa_{1-x}Fe_xSe_2$ single crystal. We carried out initial structure optimizations by SIESTA [11] computer code using optimized norm-conserving pseudopotentials [12–14] and double-ζ basis set augmented by polarization orbitals (DZP). The basis functions were generated with the energy shift parameter of 50 meV, and the DFT forces were augmented by Grimme's dispersion correction [15]. The structures were optimized in conjugate gradient algorithm until all force components were less than 0.04 eV/Å. The electronic and magnetic structure of the relaxed systems were calculated in OpenMX code using norm-conserving pseudopotentials [16,17], and pseudo-atomic localized basis functions [18,19]. Our calculations correspond to scaler relativistic treatment of collinear spins. Dudarev's GGA+U method [20] with the *U* value of 4.0 eV for Fe 3d was utilized in both SIESTA structure optimization and OpenMX magnetic structure calculations. In the Brillouin zone of our rather large supercell, a k-point sampling of 5×5×5 was utilized. The electronic temperature was set to 300 K, and the charge density was expressed on a real space grid corresponding to 220 Ry plane wave cutoff. We calculated effective exchange coupling parameters J_{ij} between atoms i and j based on Green's function representation of Liechtenstein formula [21] using 'jx' post-processing code in OpenMX version 3.9 program package [22,23]. We used a denser k-point mesh of 20×20×20 in the post-processing stage of our exchange coupling calculations.

3. RESULTS AND DISCUSSION

The results of EDX analysis of $TlGa_{1-x}Fe_xSe_2$ are shown in Fig. 2. EDX spectra were collected and used to determine the presence and average Tl, Ga, Se elements concentration as well as nominal degree of Fe substitution in individual crystals. EDX elemental mapping collected from different samples and different regions within individual crystals confirmed the presence of constituted atoms Tl/Ga/Se with atomic ratio nearly close to stoichiometric ones 1:1:2. For $TlGa_{1-x}Fe_xSe_2$ single crystal with $x = 0.023$, the real atomic composition ratio of constituent elements Tl/Ga/Se/Fe was detected as 20.57:32.14:46.54:0.75 at %, respectively. The elemental maps obtained from EDX studies showed that both of $TlGa_{1-x}Fe_xSe_2$ samples have a deficit of Tl and Se atoms and an excess of Ga atoms with respect to the stoichiometric composition. It is worth noting that there are no additional peaks corresponding to other impurities or contaminants, which confirms the high purity of the prepared single crystal.

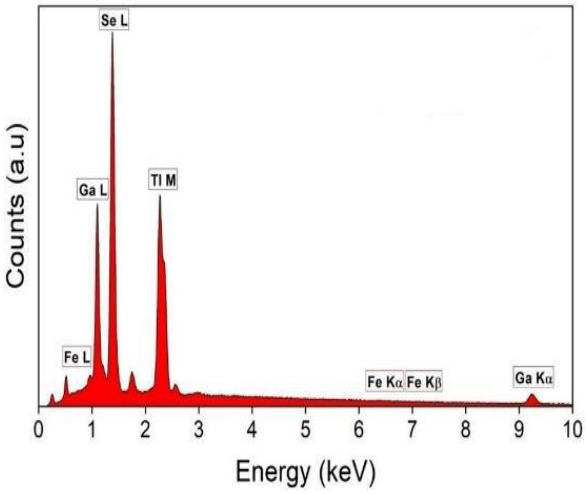

Fig.2. The results of the EDX analysis of $TlGa_{0.977}Fe_{0.023}Se_2$ crystal

The temperature dependencies of mass magnetic susceptibilities $\chi(T)$ of $TlGa_{1-x}Fe_xSe_2$ measured in ZFC and FC regimes in the temperature range from ~ 10 to ~ 400 K are shown in Fig. 3. The data were taken in an external dc magnetic field of H = 50 Oe applied to samples in two geometries: parallel ($H_{\parallel}$) and perpendicular ($H_{\perp}$) to the sample surface (ab). At high

temperatures well above ~ 250 K, the Curie – Weiss - like temperature dependences are observed in $\chi(T)$ for $H_{\parallel}$ and $H_{\perp}$. The shape of the $\chi(T)$ curves presented in Fig. 3 indicates the presence of not only both paramagnetic and diamagnetic contributions but also the small long - range ferromagnetic (or antiferromagnetic) one, which becomes most noticeable at temperatures corresponding to a broad maximum of $\chi(T)$ observed for parallel and perpendicular orientations at T_{max} ~ 170 and 155 K, respectively. Thus, the total magnetic susceptibilities of samples represent the sum of the paramagnetic and ferromagnetic (antiferromagnetic) components with the ferromagnetic contribution is rather small than the paramagnetic one.

It should be mentioned that the pristine $TlGaSe_2$ single crystal is a semi – insulating semiconductor which is known to contain several discrete native deep acceptor levels distributed inside the band gap near above the valence band maximum [24]. On the other hand, native deep acceptors are compensated by the shallow donor levels which existed in the energy gap of the undoped $TlGaSe_2$ [25,26]. As a result, $TlGaSe_2$ compound is deeply compensated semiconductor with an extremely low bulk majority charge carrier concentration and poor transport kinetics [27]. For example, the resistivity of $TlGaSe_2$ single crystal at room temperature is in the ~ 10^8-10^{10} $\Omega \cdot$ cm range [28]. Obviously, no Pauli paramagnetic contribution from conduction electrons to the temperature dependence of the magnetic susceptibility should be expected. We believe that the magnetic Fe atoms are a single source of paramagnetism in $TlGa_{1-x}Fe_xSe_2$. It is conceivable that the Fe atoms are inhomogenously distributed inside of both sample forming local Fe - rich clusters (domains) coexist with paramagnetic Fe - poor areas (less than statistically one Fe^{3+} ion per site). It is possible to conclude with certainty that Fe - poor areas form the paramagnetic matrix in $TlGa_{1-x}Fe_xSe_2$. It is obvious that magnetic properties cannot be rigorously approximated using the Curie - Weiss law. However, we will use the Curie - Weiss approximation for experimentally derived temperature dependences of magnetic susceptibility of $TlGa_{1-x}Fe_xSe_2$ for evaluating some magnetic parameters.

Above T_{max}, the magnetization curves of both samples can be satisfactory fitted with the Curie - Weiss law [29–31]:

$$[\chi(T)]^{-1} = \frac{(T-\Theta_{CW})}{C} \quad , \qquad (1)$$

where Θ_{CW} is the Curie - Weiss temperature, T is the absolute temperature and C is the Curie constant. Fig. 3 illustrates these behaviors by showing the temperature dependence of the reciprocal susceptibility (χ^{-1}) versus temperature. The magnetic behavior exhibited almost Curie - Weiss behavior (1) in temperature range above ~ 250 K. The Curie - Weiss temperature was estimated as ~ 380 K for $H_{\parallel}$ and ~ 255 K for $H_{\perp}$ measuring geometries.

The fact that magnetic behavior of $TlGa_{1-x}Fe_xSe_2$ are completely come from the Fe atoms suggesting that the Weiss molecular - field theory [32] (related to the interactions between total magnetic moment of the isolated Fe atom with its neighbors may be replaced by an effective magnetic field called as the Weiss molecular field) may be qualitatively applied for estimating some quantities related to the interacting magnetic Fe atoms. From the slope C of the linear Curie - Weiss fitting, the effective magnetic moment (per formula unit) $TlGa_{1-x}Fe_xSe_2$ semiconductors originated from Fe^{3+} – spin states can be estimated through the well - known relations [29–31]:

$$\mu_{\text{eff}} = \left(\frac{3k_BC}{N_A}\right)^{1/2} \quad , \qquad (2)$$

where k_B is the Boltzmann constant, N_A is the Avogadro number. A magnetic moment of Fe^{3+} ion in the high - spin S = 5/2 state is $\mu = g_{Fe}\sqrt{S(S+1)}\mu_B \sim 5.93\ \mu_B$. Here, μ_B is the Bohr magneton number and g_{Fe} is the Lande gyromagnetic factor, which is approximately equal to ~ 2 for Fe^{3+} ion in the $1s^22s^22p^63s^23p^63d^5$ electron configurations. Using values for μ_{eff} and experimental fitting parameters (C and Θ_{CW}) one can calculate the effective exchange interaction parameter given by the following equation [29–31]:

$$\frac{J_{ex}}{k_B} = \frac{3\Theta_{CW}}{2\langle x\rangle S(S+1)Z_{N-N}} \quad , \qquad (3)$$

where $\langle x\rangle$ is the average atomic fraction of the magnetic Fe^{3+} ions in $TlGa_{1-x}Fe_xSe_2$ samples which contribute to ferromagnetism and Z_{N-N} is the minimum number of Fe^{3+} nearest neighbor magnetic impurities incorporated into cation sites of host material which may provide an effective magnetic moment due to parallel alignment of interacting the Fe^{3+} $3d$ electron spins. In Eq. (3), $\langle x\rangle$ value in the denominator can be estimated from [29–31]:

$$\langle x\rangle = \frac{M_{Tl}+M_{Ga}+M_{Se}}{S(S+1)[g_{Fe}\mu_B]^2/(3\Theta_{CW}k_B)+M_{Se}-M_{Fe}} \qquad (4)$$

where M_{Tl}, M_{Ga}, M_{Se} and M_{Fe} are the atomic masses of the thallium, gallium cation atoms, selenium anion atom and iron magnetic impurity, respectively.

The calculated average values of J_{ex}/k_B were found to be positive, which confirm our assumption about a weak ferromagnetic ordering in $TlGa_{1-x}Fe_xSe_2$ at temperatures above ~ 250 K.

It can be seen from the plots of the inverse magnetic susceptibility χ^{-1} versus T that there is a significant temperature range ($T \lesssim 250$ K) over which the Curie constant (the slope of $\chi^{-1}(T)$ curve) of $TlGa_{1-x}Fe_xSe_2$ are almost zero for $H_{\parallel}$ orientation, which suggests that all the Fe^{3+} spins are almost paired. This result is unexpected since at higher temperatures the magnetic ordering in $TlGa_{1-x}Fe_xS_2$ samples are expected as a weak ferromagnetic.

On the other hand, from the magnetic susceptibility data plotted in Fig. 3 (that is the shape of susceptibility curves and the minima in the inverse

susceptibility $1/\chi$ vs. T plot) one can assume that the antiferromagnetic contributions from Fe^{3+} impurity moments to the magnetic susceptibility at low temperatures also take place. The data in Fig. 3 clearly show that as the temperature is decreased the χ(T) curves demonstrate the broad maximum inherent probably to the antiferromagnetic transition at T_{max} in both samples [33]. Interestingly, the FC and ZFC magnetization curves for $TlGa_{1-x}Fe_xSe_2$ nearly merged in the temperature range from ~ 400 K (the starting temperature of the experiment) to T_{max} and they start to differ faintly at cooling below T_{max} as evident from Fig. 3. Another interesting phenomenon is an absence the bifurcation in the behaviors of FC and ZFC branches at $T \leq T_{max}$.

Additionally, no bifurcation between FC and ZFC data suggests the presence of quasi - two - dimensional short - range spin – spin interatomic correlations between Fe^{3+} ions [34] which determinates non - linearity in $1/\chi$(T) behavior in the temperature ranges below ~ 250 K.

To complete the investigation of the magnetic properties of $TlGa_{1-x}Fe_xSe_2$, the magnetization (M) versus H curves were measured at various temperature in the magnetic fields up to ~ 50 kOe by a step – by - step increase of H, keeping the speed of the applied field at constant value. The temperature was stabilized at each measuring temperature to within of $\pm\, 10^{-2}$ K.

Fig. 4 demonstrate a set of M - H curves taken at various temperatures on heating regime. As seen from the figure, the sample exhibits three contributions to the magnetization, namely: an intrinsic diamagnetic contribution from nonmagnetic $TlGaSe_2$ host; a paramagnetic contribution as well as a ferromagnetic contribution due to Fe metal impurities. Corrections for diamagnetic contributions to M - H curves originated from quartz sample holder and thin Teflon tape have been made.

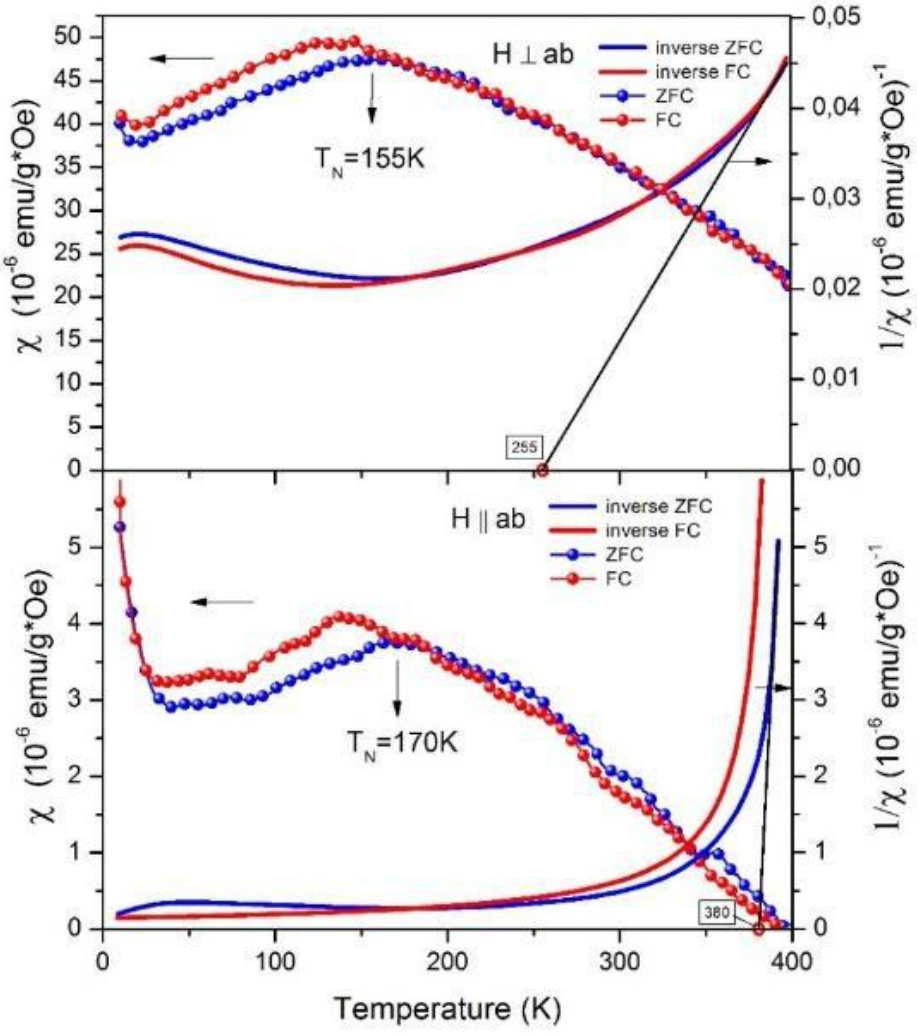

Fig. 3. Temperature dependence of FC, ZFC mass magnetic susceptibility and inverse susceptibility for $TlGa_{0.977}Fe_{0.023}Se_2$ under applied field of H = 50 Oe applied to perpendicular and parallel to *ab* - plane. Susceptibility vs temperature for both samples showing a maximum denoted by T_{max}. The blue and red colored solid circles represent ZFC and FC data, respectively. The blue and red solid line represent the inverse susceptibility of ZFC and FC measurement, respectively. The linear dashed line indicates the Curie - Weiss fit to inverse magnetic susceptibility.

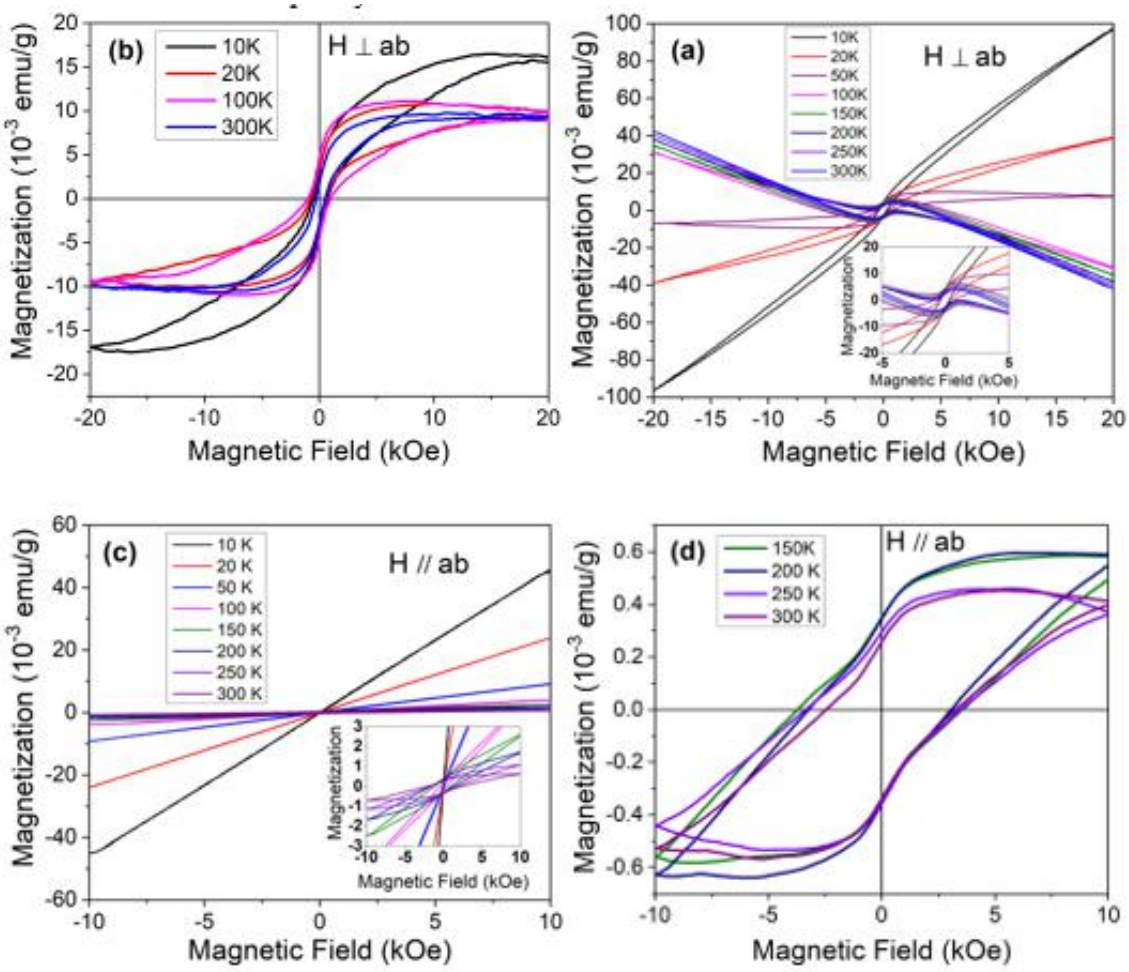

Fig. 4. M - H curves of $TlGa_{0.977}Fe_{0.023}Se_2$ sample taken at different temperatures in the range from ~ 10 to ~ 400 K for various magnetic field amplitudes changing between maximum values of $\pm$ 50 kOe. (a) –and (c) are recorded for *H* orientations applied to perpendicular and parallel to the ab – sample surface, respectively. The corresponding ferromagnetic component of some loops after subtracting diamagnetic/paramagnetic contribution are displayed in: (b) for perpendicular and (d) parallel magnetic field orientations. The insets display zoomed view of hysteresis loops with linear diamagnetic/paramagnetic contribution.

The traces of ferromagnetic - like symmetric hysteresis loop superimposed on a straight - line component with negative slope (that is typical for diamagnetic contribution) at high temperatures as well as on paramagnetic component at low temperatures are clearly observed from Fig. 4. The hysteresis loops in this figure are zoomed in magnetization scale to compare their shapes within, to some extent, low - field regions. To summarize these analysis, we can make some main conclusions: a) the paramagnetic contribution Fe^{3+} ions becomes more pronounced with decreasing temperature; b) the major part of Fe^{3+} impurities occupies Ga atomic sites are not ferromagnetically ordered; c) by subtraction of straight lines related to diamagnetic and paramagnetic contributions from the data presented in Fig. 4, clear ferromagnetic - like hysteresis loops with well - defined coercive field (H_c) and saturation magnetization (M_s) can be observed over all temperatures.

Fig. 4 shows magnetic hysteresis loops $TlGa_{1-x}Fe_xSe_2$ with $x = 0.023$ in out of ab - plane applied magnetic field geometry corrected by the diamagnetic and paramagnetic contributions as a function of temperature. The saturation magnetization of sample at ~ 10 K is found to be about 16.4×10^{-3} emu/g, that is much higher than the values at higher temperatures. The interesting phenomenon observed in Fig. 4 is that the M – H magnetic hysteresis loops have a slightly wasp waisted loop (or pinched off) character which may be related to the antiferromagnetic interaction between some and Fe^{3+} ions.

Similar modulation in magnetic hysteresis loops is also observed for $TlGa_{1-x}Fe_xSe_2$ measured along the direction parallel to ab – surface plane at various temperatures (see Fig. 4 (d)). As it is clearly seen from this figure, a very wide and almost rectangular in shape magnetic loops with weakly pinched off at the center exhibiting remarkably high coercivities and quite low M_s values were recorded for $TlGa_{1-x}Fe_xSe_2$ especially above ~ 150 K. This behavior may be explained by a reversible motion of a small micro - domain like elements around the individual Fe^{3+} ion requiring stronger magnetic fields for remagnetization. Thus, based on our experimental findings, a possible scenario for magnetic ordering in $TlGa_{1-x}Fe_xSe_2$ can be suggested. A combination of two independent types of magnetic interactions between trivalent iron impurities introduced into nonmagnetic host lattice positions,

namely, a weak ferromagnetic ordering and antiferromagnetic coupling may be responsible for the magnetic ordering in $TlGa_{1-x}Fe_xSe_2$. Depending on the x parameter, the dominant magnetic state between randomly located impurity local moments in $TlGa_{1-x}Fe_xSe_2$ may be ordered either in a long – range ferromagnetic state or a short - range antiferromagnetic one. In addition, due to local fluctuations of Fe concentration in the host lattice structure of $TlGaSe_2$, Fe - poor areas the paramagnetic matrix

Let us to discuss our model of Fe-doped $TlGaSe_2$ crystal structure suggested for description of magnetic data. We have considered a model $TlGa_{1-x}Fe_xSe_2$ structure presented in Fig. 1, in which $GaSe_4$ polyhedrons are indicated by the green color, and $FeSe_4$ ones are colored by the red. We used a 128-atom supercell of $TlGaSe_2$ as the unit cell in our calculations, and a Ga atom in the unit cell was substituted by a Fe atom. Our model system corresponds to x = 0.03125 in $TlGa_{1-x}Fe_xSe_2$, where the separation between Fe dopants is larger than 15 Å. To access smaller Fe - Fe distance values for exchange coupling calculations we calculated substitutional double - doped systems.

The structure shown in Fig. 1 was fully relaxed without any symmetry constraints. The substitution does not induce notable structural modifications, and the dopant makes four equal - length Fe - Se bonds of $\cong$ 2.4 Å. The system remains semiconducting after the single Fe substitution at the Ga site that corresponds to low doping levels. From our DFT modeling we find that the spin polarization per Fe dopant to be 5 μ_B, which corresponds to S = 5/2 for the collinear spin case. This value is nearly consistent with that reported above (5.93 μ_B). Both SIESTA and OpenMX codes give the same magnetic structure. To make sure that our results are not affected by localized basis sets we verified the total magnetic moment by plane wave basis set calculations with Quantum - Espresso computer code [35]. The net spin density $\rho(\uparrow) - \rho(\downarrow)$, defined as the density of majority electrons minus the minority electrons, is depicted as 3D isosurface in Fig. 5, where the density difference $\rho(\uparrow) - \rho(\downarrow)$ is 0.004 electron/bohr^3. The net spin is distributed over the Fe dopant and its neighboring Se atoms, which form the Fe-centered polyhedron. The other atoms in the unit cell have negligible net spin values. The effective exchange coupling J values between the atoms with localized spins are listed in Table 1 as a function of interatomic distances. The exchange coupling $J_{\text{Fe-Se}}$ between the Fe dopant and Se atoms in the unit cell, provided in the left half of Table 2, indicate a ferromagnetic coupling between Fe and Se.

The exchange coupling between Fe - Fe dopants denoted as $J_{\text{Fe-Fe}}$ and listed in the right half of Table 2, indicates antiferromagnetic coupling between Fe dopants. Note that there are two Fe dopants in the unit cell for the distances smaller than 15 Å. At the Fe - Fe distance value of 3.91 Å, there is a bridging Se atom between two Fe dopants. The $J_{\text{Fe-Fe}}$ value of -119 meV for this configuration indicates that Se atoms mediate the antiferromagnetic coupling in the system. The exchange coupling $J_{\text{Fe-Fe}}$ decreases with distance but remains negative. The $J_{\text{Fe-Fe}}$ value for 15.5 Å is essentially the coupling between the Fe dopants in neighboring unit cells of $TlGa_{1-x}Fe_xSe_2$ for x=0.03125. The relevant exchange coupling scale between Fe dopants in our system is $J_{\text{Fe-Fe}} = -0.261$ meV since our doping levels are low enough to rule out smaller Fe separations. The electronic and magnetic coupling between the layers is weak, and there are four nearest Fe dopant in a layer. Therefore, the effective exchange coupling experienced by an Fe dopant is approximately -1.0 meV for low doping levels.

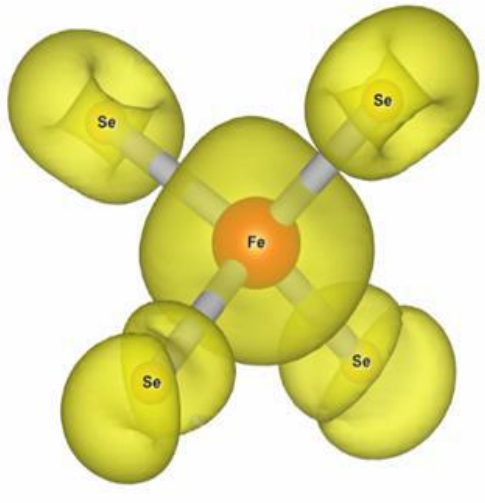

Fig. 5. View of the spin polarization around the single Fe – substituted atom epresented as an isosurface, where the net spin density $\rho(\uparrow) - \rho(\downarrow)$ is 0.004 electron/bohr^3.

The magnetic coupling extends beyond the direct exchange spatial separation range. However, $J_{\text{Fe-Se}}$ beyond the lattice length of 15.48 Å is negligibly small.

Table 1.
Effective exchange coupling between localized spins as a function of distance. $J_{\text{Fe-Se}}$ is the coupling between Fe and Se atoms, $J_{\text{Fe-Fe}}$ between Fe atoms.

distance (Å)	$J_{\text{Fe-Se}}$ (meV)	distance (Å)	$J_{\text{Fe-Fe}}$(meV)
2.41	21.8	3.91	-119
5.98	0.180	7.74	-9.97
9.76	0.0123	15.5	-0.261

Thus, in Fe-doped $TlGaSe_2$, an Fe dopant has ferromagnetic coupling with Se atoms and antiferromagnetic coupling with other Fe dopants. As the exchange coupling decreases with distance, the effective Fe-Se exchange coupling is stronger than Fe-Fe coupling for low doping levels.

4. CONCLUSION

A novel $TlGa_{1-x}Fe_xSe_2$ layered magnetic semiconductors diluted with 3 d iron impurities with doping ratio of 2.3 % were grown by using Bridgman - Stockbarger method. The positive value of θ_{CW} obtained from antiferromagnetic curve deduced from VSM magnetic susceptibility χ (T) measurement has been extracted. The obtained hysteresis loops prove the existence of ferromagnetic structure. Through first - principles theoretical calculations, we explore that the $TlGa_{1-x}Fe_xSe_2$ compound shows a weak antiferromagnetic order via Fe - Fe linkages

and ferromagnetic coupling via Fe−Se linkages within the layers. There is also a paramagnetic component in $TlGa_{1-x}Fe_xSe_2$ which likely arises from the Fe - poor regions. Thus, the Fe - Fe and Fe - Se bond lengths may play an important role in magnetic ordering of $TlGa_{1-x}Fe_xSe_2$ magnetic semiconductor

[1] *G.A. Prinz,* Magnetoelectronics, Science, 282 (1998) 1660–1663.

[2] *H. Ohno,* Making nonmagnetic semiconductors ferromagnetic, Science, 281 (1998) 951–956.

[3] *S.A. Wolf, D.D. Awschalom, R.A. Buhrman, J.M. Daughton, von S. von Molnár, M.L. Roukes, A.Y. Chtchelkanova, D.M. Treger,* Spintronics: a spin-based electronics vision for the future, Science, 294 (2001) 1488–1495.

[4] *Y. Matsumoto, M. Murakami, T. Shono, T. Hasegawa, T. Fukumura, M. Kawasaki, P. Ahmet, T. Chikyow, S. Koshihara, H. Koinuma,* Room-temperature ferromagnetism in transparent transition metal-doped titanium dioxide, Science, 291 (2001) 854–856.

[5] *D. Müller, H. Hahn,* Untersuchungen über ternäre Chalkogenide. XXIV. Zur Struktur des $TlGaSe_2$, Zeitschrift Für Anorg. Und Allg. Chemie. 438 (1978) 258–272.

[6] *A. Cengiz, Y.M. Chumakov, M. Erdem, Y. Şale, F.A. Mikailzade, M.Y. Seyidov,* Origin of the optical absorption of $TlGaSe_2$ layered semiconductor in the visible range, Semicond. Sci. Technol. 33 (2018) 75019.

[7] *S. Yang, M. Wu, H. Wang, H. Cai, L. Huang, C. Jiang, S. Tongay,* Ultrathin ternary semiconductor $TlGaSe_2$ phototransistors with broad-spectral response, 2D Mater. 4 (2017) 35021.

[8] *W. Kohn, L.J. Sham,* Self-consistent equations including exchange and correlation effects, Phys. Rev. 140 (1965) A1133.

[9] *P. Hohenberg, W. Kohn,* Inhomogeneous electron gas, Phys. Rev. 136 (1964) B864.

[10] J.P. Perdew, K. Burke, M. Ernzerhof, Generalized gradient approximation made simple, Phys. Rev. Lett. 77 (1996) 3865.

[11] J.M. Soler, E. Artacho, J.D. Gale, A. García, J. Junquera, P. Ordejón, D. Sánchez-Portal, The SIESTA method for ab initio order-N materials simulation, J. Phys. Condens. Matter. 14 (2002) 2745.

[12] D.R. Hamann, Optimized norm-conserving Vanderbilt pseudopotentials, Phys. Rev. B. 88 (2013) 85117.

[13] D.R. Hamann, Erratum: optimized norm-conserving vanderbilt pseudopotentials, Phys. Rev. B 88, 085117 (2013)], Phys. Rev. B. 95 (2017) 239906.

[14] M. Schlipf, F. Gygi, Optimization algorithm for the generation of ONCV pseudopotentials, Comput. Phys. Commun. 196 (2015) 36–44.

[15] S. Grimme, Semiempirical GGA-type density functional constructed with a long-range dispersion correction, J. Comput. Chem. 27 (2006) 1787–1799.

[16] I. Morrison, D.M. Bylander, L. Kleinman, Nonlocal Hermitian norm-conserving Vanderbilt pseudopotential, Phys. Rev. B. 47 (1993) 6728.

[17] [N. Troullier, J.L. Martins, Efficient pseudopotentials for plane-wave calculations, Phys. Rev. B. 43 (1991) 1993.

[18] T. Ozaki, Variationally optimized atomic orbitals for large-scale electronic structures, Phys. Rev. B. 67 (2003) 155108.

[19] T. Ozaki, H. Kino, Numerical atomic basis orbitals from H to Kr, Phys. Rev. B. 69 (2004) 195113.

[20] *S.L. Dudarev, G.A. Botton, S.Y. Savrasov, C.J. Humphreys, A.P. Sutton,* Electron-energy-loss spectra and the structural stability of nickel oxide: An LSDA+ U study, Phys. Rev. B. 57 (1998) 1505.

[21] *A. Il Liechtenstein, M.I. Katsnelson, V.P. Antropov, V.A. Gubanov,* Local spin density functional approach to the theory of exchange interactions in ferromagnetic metals and alloys, J. Magn. Magn. Mater. 67 (1987) 65–74.

[22] *M.J. Han, T. Ozaki, J. Yu,* Electronic structure, magnetic interactions, and the role of ligands in Mn n (n= 4, 12) single-molecule magnets, Phys. Rev. B. 70 (2004) 184421.

[23] *A. Terasawa, M. Matsumoto, T. Ozaki, Y. Gohda,* Efficient algorithm based on liechtenstein method for computing exchange coupling constants using localized basis set, J. Phys. Soc. Japan. 88 (2019) 114706.

[24] *M.Y. Seyidov, Y. Sahin, M.H. Aslan, R.A. Suleymanov,* Mechanisms of current flow in p-$TlGaSe_2$ single crystals, Semicond. Sci. Technol. 21 (2006) 1633.

[25] *M.Y. Seyidov, F.A. Mikailzade, T. Uzun, A.P. Odrinsky, E. Yakar, V.B. Aliyeva, S.S. Babayev, T.G. Mammadov,* Identification of intrinsic deep level defects responsible for electret behavior in $TlGaSe_2$ layered semiconductor, Phys. B Condens. Matter. 483 (2016) 82–89.

[26] *M.Y. Seyidov, R.A. Suleymanov, E. Balaban, Y. Şale,* Imprint electric field controlled electronic transport in $TlGaSe_2$ crystals, J. Appl. Phys. 114 (2013) 93706.

[27] *M.Y. Seyidov, Y. Sahin, D. Erbahar, R.A. Suleymanov,* Electret states and current oscillations in the ferroelectric semiconductor $TlGaSe_2$, Phys. Status Solidi. 203 (2006) 3781–3787.

[28] *A.K. Fedotov, M.I. Tarasik, I.A. Svito, P. Zhukowski, T.N. Koltunowicz, T.G. Mammadov, M.Y. Seyidov, R.A. Suleymanov, V. Grivickas, V. Bicbaevas,* Electrical properties of the layered

single crystals $TlGaSe_2$ and $TlInS_2$, (2012).

[29] *J.M.D. Coey,* Magnetism and magnetic materials, Cambridge university press, 2010.

[30] *B.D. Cullity, C.D. Graham,* Introduction to Magnetic Materials, A John Wiley & Sons, 2nd Edit., 2009.

[31] *J.K. Furdyna, J. Kossut,* Eds Semiconductors and Semimetals vol. 25 (Boston: Academic) Furdyna JK 1988 J, 1988.

[32] *D.C. Mattis,* Theory Of Magnetism Made Simple, The: An Introduction To Physical Concepts And To Some Useful Mathematical Methods, World Scientific Publishing Company, 2006. https://doi.org/10.1142/5372.

[33] *J.C. Bonner, M.E. Fisher,* Linear magnetic chains with anisotropic coupling, Phys. Rev. 135 (1964) A640. https://doi.org/10.1103/PhysRev.135.A640.

[34] *X. Song, S.N. Schneider, G. Cheng, J.F. Khoury, M. Jovanovic, N. Yao, L.M. Schoop,* Kinetics and Evolution of Magnetism in Soft-Chemical Synthesis of $CrSe_2$ from $KCrSe_2$, Chem. Mater. 33 (2021) 8070–8078. https://doi.org/10.1021/acs.chemmater.1c02620

[35] *P. Giannozzi, S. Baroni, N. Bonini, M. Calandra, R. Car, C. Cavazzoni, D. Ceresoli, G.L. Chiarotti, M. Cococcioni, I. Dabo,* QUANTUM ESPRESSO: a modular and open-source software project for quantum simulations of materials, J. Phys. Condens. Matter. 21 (2009) 395502.